SCIENCE CHINA
Chemistry

• ARTICLES •

May 2015 Vol.58 No.5: 850–857
doi: 10.1007/s11426-014-5237-1

Triblock copolymer-assisted construction of 20 nm-sized ytterbium-doped TiO_2 hollow nanostructures for enhanced solar energy utilization efficiency

Lin Cheng[1,2], Xuefeng Xu[1], Yuyan Fang[1], Yan Li[1], Jiaxi Wang[1], Guojia Wan[1], Xueying Ge[1], Liangjie Yuan[1], Keli Zhang[1], Lei Liao[2*] & Quan Yuan[1*]

[1]*Key Laboratory of Analytical Chemistry for Biology and Medicine, Ministry of Education; College of Chemistry and Molecular Sciences, Wuhan University, Wuhan 430072, China*
[2]*Key Laboratory of Artificial Micro- and Nano-structures, Ministry of Education; Department of Physics, Wuhan University, Wuhan 430072, China*

Received May 13, 2014; accepted June 3, 2014; published online March 3, 2015

Rare-earth doped titania single-crystalline hollow nanoparticles of 20 nm are constructed via a simple sol-gel process. Amphiphilic ABA tri-block copolymers played a key role in assisting the formation of hollow structure, for which a hollow nanostructure growth mechanism is proposed. By introducing rare earth into the synthesis process, the as-prepared nanoparticles exhibit near-infrared light absorption properties. Photo-decomposition efficiency of Orange II azo dye can be successfully evaluated when using Yb^{3+}-doped TiO_2 hollow nanoparticles as photocatalysts; it is more than two times higher than the pure TiO_2 hollow nanoparticles. The hollow nanostructured Yb^{3+}-doped TiO_2 samples are exploited as photoanodes in N719-sensitized solar cells and prove able to improve the photoelectric conversion efficiency by measuring the solar cell parameters of dye-sensitized solar cells (DSSCs) under simulative sunlight.

rare earth, hollow nanostructure, titania, single-crystalline, copolymer

1 Introduction

Because humans have a stronger appetite for energy than ever, and because traditional fossil fuels are dirty and there are not enough to satisfy demand, finding alternatives to fossil fuels is one of the most important and urgent tasks for scientists of this century and possibly many centuries to come. Solar energy, which has always been a star in the category of clean energy, will be there as long as the sun rises; the only problem is how to turn that huge amount of energy into use. The utilization of solar energy has been widely investigated [1–5]. TiO_2, as one of the most promising and suitable semiconductor materials, has received increasing attention from all over the world for its wide potential applications in solar energy conversion in, for example, dye-sensitized solar cells (DSSCs) [6,7] and as an efficient photocatalyst [8,9]. However, its practical applications are hindered by low photon-conversion efficiency due to the rapid recombination of electron/hole caused by surface traps on the TiO_2 and limited light absorption because of its large band gap (3.2 eV).

In order to inhibit the rapid recombination of electron/hole and to enhance the light absorption of TiO_2 for solar energy applications, numerous methods have been investigated. Of these two have been widely practiced. One effective strategy involves transition metals doping [10,11] for enhanced light-absorption capacity and improved quantum yields. Rare-earth metals as dopants have recently shown great potential [12,13]. Stucky *et al*. [14] found that

*Corresponding authors (email: liaolei@whu.edu.cn; yuanquan@whu.edu.cn)

mesoporous titania doped with europium ions produced a bright near-monochromatic red luminescence because the anatase nanocrystallites excitation within their band gap resulted in nonradiative energy transfer to the europium ions. Wang *et al*. [15] and Yan *et al*. [15,16] introduced Eu^{3+}, Sm^{3+}, and Yb^{3+}. Rare-earth metals with rich spectroscopic properties can thus be doped in TiO_2 to assist the electron/energy transfer processes and suppress the recombination of electron/hole in order to increase photoconversion efficiency [17,18].

Another generally used protocol is the creation of nanostructured TiO_2 [19,20] that can achieve better solar energy applications. Of these, hollow nanostructures are of great interest in a wide range of areas (e.g., as catalysis and in energy-storage applications) due to their unique structural features. At present, hollow-structured TiO_2 has attracted much more attention because, compared to solid materials, this structure exhibits stronger light-harvesting capacity and outstanding photoelectric performance due to good permeation, high mobility, and large specific surface area [21,22]. Many efforts have been made to improve the design and synthesis of TiO_2 hollow structure. To this end, various synthesis methods for TiO_2 hollow structure have been developed, mainly templating synthesis [23,24], sacrificial templating synthesis [25], and template-free methods [26]. Lou *et al*. [27] reported the preparation of nonspherical anatase TiO_2 hollow colloids through hydrothermal deposition of polycrystalline anatase TiO_2 on six different types of hematite nanotemplates. Yang *et al*. [28] successfully fabricated anatase TiO_2 hollow spheres with diameters of 0.2–1.0 μm, in which Ostwald ripening was used to form hollow structure by hydrothermally heating a TiF_4 solution. Although various syntheses of submicrometer titania hollow structure have been reported, few works have presented the formation of TiO_2 hollow nanoparticles of less than 30 nm using a soft template method.

We report a simple and facile sol-gel process to synthesize Yb^{3+}-doped TiO_2 single-crystalline hollow nanoparticles (HNPs) about 20 nm in diameter. Our method integrates rare-earth ion doping and hollow nanostructured TiO_2 fabrication design to achieve a rationale for enhanced solar-energy utilization efficiency. Amphiphilic surfactant poly(ethylene glycol)-block-poly(propylene glycol)-block-poly(ethylene glycol) (P123) as the templating agent plays an important role in directing the formation of hollow structure. By doping rare-earth metal ions, the obtained crystallized ytterbium-doped TiO_2 HNPs exhibit near-infrared light-absorption properties. We further investigated the photocatalytic efficiency of the products by using Orange II dye degradation as probe reaction, and found that after irradiating for 160 min, 86% of the Orange II was decomposed on the Yb^{3+}-doped TiO_2 HNPs whereas 40% of the dye was degraded on the pure TiO_2 HNPs. The photoelectric conversion efficiency was also improved via exploiting the HNPs as photoanodes in DSSCs. The DSSC with 0.5 mol% Yb^{3+}-doped TiO_2 HNPs achieved a maximum short-circuit photocurrent density of 7.63 mA/cm^2 and energy-conversion efficiency of 3.66%, which is much better than pure TiO_2 hollow nanoparticles.

2 Experimental

2.1 Materials

Pluronic P123 (M_{av}=5800, $EO_{20}PO_{70}EO_{20}$) was purchased from Sigma-Aldrich (US). Hydrochloric acid, ethanol, Yb_2O_3, and $TiCl_4$ were purchased from Sinopharm Chemical Reagent Co. (China). All other chemicals were used as received.

2.2 Synthesis of $YbCl_3 \cdot 6H_2O$

First, Yb_2O_3 (2.5 mmol) and hydrochloric acid (15 mmol) were added into 50 mL of deionized water with stirring and the mixture was heated to 120 °C. After the solution became clear, heating was stopped and then the solution was cooled to room temperature. This resulting solution was evaporated to get crystals in a fume hood and then dried at 60 °C overnight.

2.3 Synthesis of TiO_2 HNPs

In a typical synthesis, 1 g of Pluronic P123 was dissolved in a beaker containing 20 mL ethanol. To this solution, 2.2 mL of the anhydrous inorganic chloride precursor $TiCl_4$ was added with vigorous stirring (caution should be taken because most of these inorganic chlorides react violently with alcohol). After being stirred for 10 h at room temperature with PE film sealing the beaker, the resulting solution was aged at 40 °C for 3 days. The as-made bulk samples were then calcined at 500 °C for 4 h to remove the block copolymer surfactant.

2.4 Synthesis of ytterbium-doped TiO_2 HNPs

Ytterbium-doped TiO_2 HNPs were prepared via a method similar to the non-ytterbium-doped TiO_2 preparation process described above. Hydrous ytterbium(III) chloride ($YbCl_3 \cdot 6H_2O$) with different doping ratios (0.1 mol%, 0.5 mol%, 1 mol%, 5 mol%) was added to the ethanol solution of P123 before $TiCl_4$. Other procedures were the same as above.

2.5 Synthesis of TiO_2-noP123

2.2 mL of the anhydrous inorganic chloride precursor $TiCl_4$ was added in a beaker containing ethanol (20 mL) with vigorous stirring. The followed processes were the same as that described above.

2.6 Degradation of Orange II

First, 5 mg samples of TiO_2 HNPs with different doping ratios were dispersed into 50 mL containers of Orange II aqueous solution (10 mg/L) and the degradation processes were performed in a SGY-IB photochemical reaction instrument (Nanjing Stonetech Electric Equipment Co., Ltd., China). A 500 W xenon lamp was used as an irradiation source. At given time intervals (20 min), the supernate was analyzed by recording the variations of the absorption band maximum (484 nm) on a UV-2550 spectrometer (Shimadzu, Japan).

2.7 Preparation of photoanodes

First, 1.0 g TiO_2 samples containing different doping ratios (0 mol%, 0.1 mol%, 0.5 mol%, 1 mol%, 5 mol%) were mixed, respectively, with ethanol (8.0 mL), acetic acid (0.2 mL), terpinol (3.0 g), and ethyl cellulose (0.5 g). Then the mixture was ball-milled for 10 h to obtain homogeneous TiO_2 paste. The doctor-blading technique was used to spread the obtained paste onto a clean fluorine-doped tin oxide (FTO) substrate (15 Ω/sq). Two parallel adhesive tapes (approximately 50 μm) serving as spacers were used to control film thickness. After being dried in air, the binders in the paste were removed by sintering the film at 500 °C for 1 h. The electrodes were immersed overnight in an ethanol solution containing 0.3 mmol/L N719 dye to achieve dye sensitization and then washed with ethanol and dried in dry air.

2.8 Assembly of dye-sensitized solar cell

These dye-sensitized electrodes were assembled into two-electrode sandwich cells. The composition of the iodine electrolyte was 0.5 mol/L LiI, 0.05 mol/L I_2, and 0.1 mol/L 4-*tert*-butylpyridine in 1:1 acetonitrile propylene carbonate, which was introduced into the space between the identical platinized FTO counter electrode and the photoanode.

2.9 Characterization

The morphology of the TiO_2 samples was analyzed with a JEM-2100 transmission electron microscope (JEOL, Japan). The nanostructures of the products and energy-dispersive X-ray spectroscopy (EDX) analyses were investigated with a Tecnai G^2 F20 high-resolution transmission electron microscope (FEI, US). Structure phase analyses via an X-ray diffraction method were performed on a D8-advance X-ray diffractometer (Bruker, Germany) with Cu-Kα radiation (λ=0.15418 nm) in a 2θ range from 10° to 80° at a speed of 6°/min. The UV-Vis-NIR absorption spectra were recorded on a UV-3600 spectrophotometer (Shimadzu, Japan); the powders were uniformly ground and then dry-pressed in a solid sample holder, using barium sulfate (SP) as standard. The N_2 adsorption-desorption isotherm was obtained by using a NOVA 4200e surface area & pore size analyzer (Quantachrome, US). The photodegradation processes were performed in a SGY-IB photochemical reaction instrument (Nanjing Stonetech Electric Equipment Co., Ltd., China). The current-density/voltage characteristics for the fabricated DSSCs were recorded under one-sun condition with 100 mW/cm^2 (AM 1.5 G) from a 91160 solar-light simulator (Newport, US). Electrochemical impedance spectroscopy measurements were performed at an applied bias of V_{OC} and a frequency between 0.05 Hz and 100 kHz, with alternating current (AC) amplitude of 10 mV under a simulated solar-light illumination on a CHI-604D electrochemical analyzer (Shanghai CH Instruments Inc., China). The active area was about 0.1 cm^2. Three DSSC devices were tested for each sample.

3 Results and discussion

Transmission electron microscopy (TEM) images (Figure 1(a)) show that the 0.5 mol% Yb^{3+}-doped TiO_2 HNPs calcinated at 500 °C had hollow structures. A major crystallite size is about 20 nm according to the size distribution histogram (Figure S1, Supporting Information online). A high-resolution TEM (HRTEM) image clearly illustrates the hollow nanocrystal with single-crystalline structure (Figure 1(b)). The distance between adjacent lattice fringes in the highly ordered lattice array over the shell is 0.35 nm confirmed as the standard lattice spacing of the (101) planes of anatase TiO_2 [29], which indicates the as-prepared TiO_2 HNPs are well-defined anatase crystal. High-angle annular dark-field scanning transmission electron microscopy-energy dispersive X-ray spectroscopy (HAADF-STEM-EDS) line-scan analysis (Figure 1(c)) revealed the Ti and O elements distributions in a single ytterbium-doped TiO_2 HNP, which demonstrates by scanning across the whole particle that the levels of Ti and O elements on both sides are higher than the central level, which provides more evidence for the formation of hollow structure. EDX characterization (Figure 1(d)) further determined the composition of the HNPs and confirmed the presence of Yb in the TiO_2 HNPs.

The X-ray diffraction (XRD) spectra of the TiO_2 HNPs calcinated at 500 °C with varied Yb^{3+} additions are given in Figure 2. All of the diffraction peaks match well with the characteristic anatase phase peaks (JCPDS Card No. 21-1272) and the ytterbium oxide crystalline phase is not found, which demonstrates that the as-prepared products were nanocrystals in the anatase phase. As the calcination temperature increased, the XRD signals gradually sharpened (Figure S2, Supporing Information online), which illustrates that higher temperature results in better crystallization. In order to further confirm the nanostructure of the TiO_2 HNPs, nitrogen adsorption-desorption measurements were carried

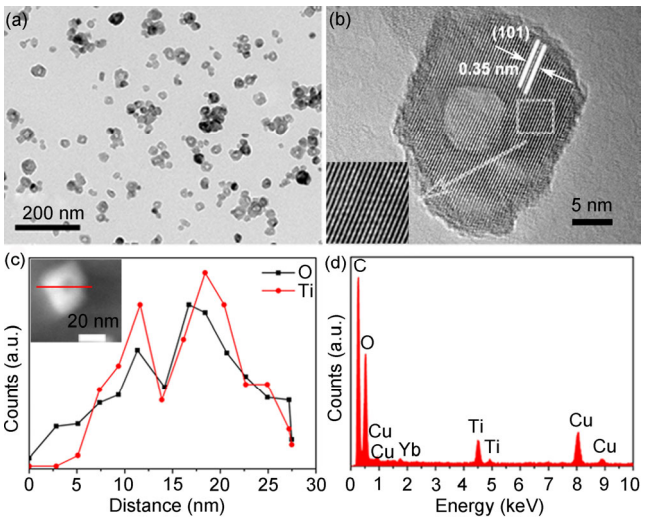

Figure 1 (a) TEM and (b) HRTEM images of 0.5 mol% Yb^{3+}-doped TiO_2 HNPs calcinated at 500 °C (the inset of (b) displays a corresponding partial, enlarged view); (c) corresponding HAADF-STEM-EDS line scan profile; (d) corresponding EDX characterization.

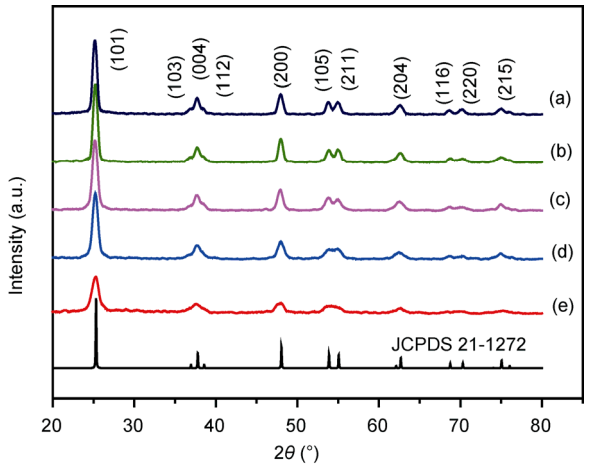

Figure 2 XRD patterns of pure TiO_2 HNPs, Yb^{3+}-doped TiO_2 HNPs with varied Yb^{3+} addition calcinated at 500 °C. (a) Pure TiO_2; (b) 0.1 mol% Yb; (c) 0.5 mol% Yb; (d) 1 mol% Yb; (e) 5 mol% Yb.

out to study the Brunauer-Emmett-Teller (BET) surface area (Figure S3, Supporing Information online). The isotherms of 0.5 mol% Yb^{3+}-doped TiO_2 HNPs can be ascribed to Type IV with H1-shaped hysteresis loops, which implies the presence of uniform hollow nanostructure. It was found that the BET surface area of 0.5 mol% Yb^{3+}-doped TiO_2 HNPs was 76 m^2/g, 73% higher than nanoparticles without hollow structure (20 m^2/g) (denoted TiO_2-noP123) (Figure S4, Supporing Information online).

Amphiphilic ABA tri-block copolymers, an important type of surfactant, have been used as a new species of additive in the synthesis of inorganic nanostuctures [30]. In our work, the small-sized TiO_2 HNPs were fabricated with $TiCl_4$ as the Ti resource; the non-ionic surfactant P123 ($EO_{20}PO_{70}EO_{20}$) was also added in the synthesis. Utilizing micelle of block polymers with metal precursor is a popular approach for the fabrication of nanostructured materials, especially in the synthesis of mesoporous nanostructure [31]. Many theories have attempted to describe the interaction between the inorganic salts and the surfactant polymer in the fabrication of mesoporous materials. In the mechanism of liquid-crystal templating presented by Beck *et al.* [32], electrostatics cause inorganic species interact with surfactant micelle. According to the charge matching at the organic-inorganic interface, a cooperative organization mechanism was proposed by Stucky *et al.* [33]. Hydrogen bonding, ligand-assisted templating, complex formation or coordinated bonding in the hydrolysis, and condensation have also been proposed based on experimental results [33,34]. The mechanism of the formation of titanium nanoparticles with hollow structure can be explained based on a series of theory models and experimental data. Here, we propose that the amphiphilic surfactant P123 can be used as the structure-directing agent to control the shape and size of particles during synthesis. The mechanism of the formation of TiO_2 HNPs presented in Scheme 1 can be divided into three steps: (1) micellization of the P123 and hydrolysis of the Ti precursor; (2) adsorption of Ti^{4+} to the hydrophilic poly(ethylene oxide) (PEO) segments of spherical P123 surfactant micelles to accomplish the condensation; (3) removal of the P123 template.

In the first step, the micellization process of P123 occurs in the presence of solvent at room temperature. In our study, according to the Lewis acid-base theory, the Ti precursor $TiCl_4$ acted as a strong Lewis acid to produce chloroalkoxide and HCl [35]. The Cl^- produced by hydrolyzation was expected to decrease the critical micellization temperature (CMT) and thus facilitate the micellization, due to Hofmeister anion effects [36–38] on surfactant self-assembly that could inhibit the formation of second-order or higher-order aggregates. In the second process, it has been well documented that multivalent metal species (including titanium species) prefer associating with hydrophilic PEO blocks instead of hydrophobic poly (propylene oxide) (PPO)

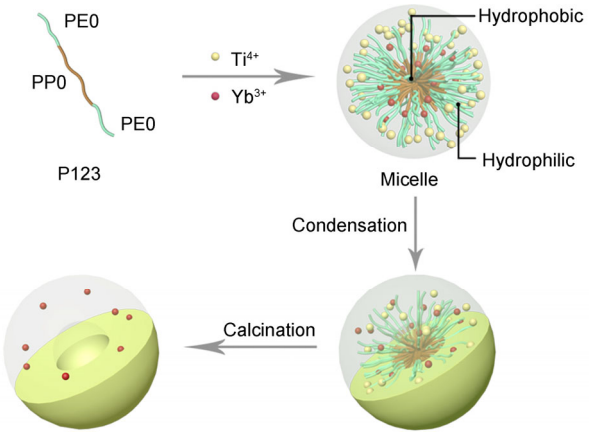

Scheme 1 Schematic illustration of the formation of Yb^{3+}-TiO_2 HNPs.

blocks, due to different binding affinities [39–41]. In fact, the surface energy of most polymers are very low; as a result, the adhesion of metals on polymers is difficult. The problem can be solved by forming specific interactions such as hydrogen bonding, chelation, or covalent bonding [30]. With the formation of crown-ether-type complexes by weak coordination bonds, the inorganic metal ions can be bound to the alkylene oxide segments (PEO) [42]. As stated in other people's study, alkylene oxide segments can form crown-ether-like complexes with cations such as metal ions [43]. In the latter process, the removal of P123 template is accomplished by the heat treatment; as a result, the hollow structured titania nanoparticles are obtained.

The UV-Vis-NIR absorption spectra of pure TiO_2 HNPs and 0.5 mol% Yb^{3+}-TiO_2 HNPs calcinated at 500 °C are shown in Figure 3. Two strong absorption bands can be seen in the UV-Vis-NIR absorption spectrum of Yb^{3+}-doped TiO_2 HNPs. The absorption band observed at about 390 nm corresponds to the TiO_2 semiconductor band gap. The other peak, in the range of 850–1050 nm, results from the 4f electron transitions of Yb^{3+} [44], while pure TiO_2 sample has no absorption in the NIR region. Orange II, a kind of azo dye, was chosen as a target of photodegradation to test the photocatalytic activity. The photodegradation of Orange II solution, triggered by pure TiO_2 HNPs and Yb^{3+}-doped TiO_2 HNPs under irradiation of a 500 W xenon lamp after absorption-desorption equilibrium in a dark room, was then monitored by a UV-Vis spectrometer. The time-dependent absorption spectra of the Orange II reaction solution in the presence of 0.5 mol% Yb^{3+}-doped TiO_2 HNPs and pure TiO_2 HNPs calcinated at 500 °C are shown in Figure 4(a) and Figure S5 (Supporting Information online), respectively. Both spectra demonstrate that the characteristic absorption strength of Orange II located at 484 nm steadily decreased with the increasing irradiation time for Orange II solution. They also clearly demonstrate that after irradiation of 160 min, 86% of Orange II was decomposed on the Yb^{3+}-doped TiO_2 HNPs, whereas 40% of dye was degraded on the pure TiO_2 HNPs. The plot of $C(t)/C(0)$ against the reaction time in the presence of 0.5 mol% Yb^{3+}-doped TiO_2 HNPs and pure TiO_2 HNPs calcinated at 500 °C are shown in Figure 4(b), where $C(t)$ is the concentration of Orange II at the irradiation time t and $C(0)$ is the original concentration. The pure TiO_2 HNPs do not show much activity compared to the blank experiment without photocatalysts. However, the as-prepared Yb^{3+}-doped TiO_2 HNPs show obviously enhanced photocatalytic activity and is more than two times higher than the pure TiO_2 HNPs. By introducing rare earth into TiO_2 HNPs, the Ti atoms could replace rare earth ions Yb^{3+} and form tetrahedral Ti sites [45]. The Ti^{4+} ion replaces a rare-earth ion with a trivalent oxidation state that leads to a charge imbalance; therefore, more hydroxide ions are adsorbed on the surface [17,18]. The hydroxide ions react with the holes generated by irradiation to form hydroxyl radicals and thereby oxidize the adsorbed molecules,

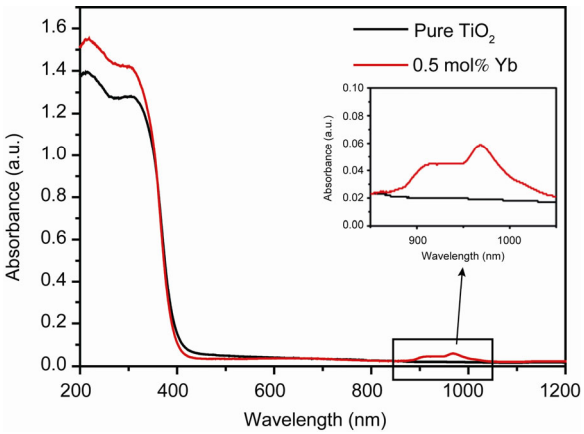

Figure 3 UV-Vis-NIR absorption of pure TiO_2 HNPs and 0.5 mol% Yb^{3+}-doped TiO_2 HNPs calcinated at 500 °C. The inset displays a corresponding, partially enlarged view from 850 to 1050 nm.

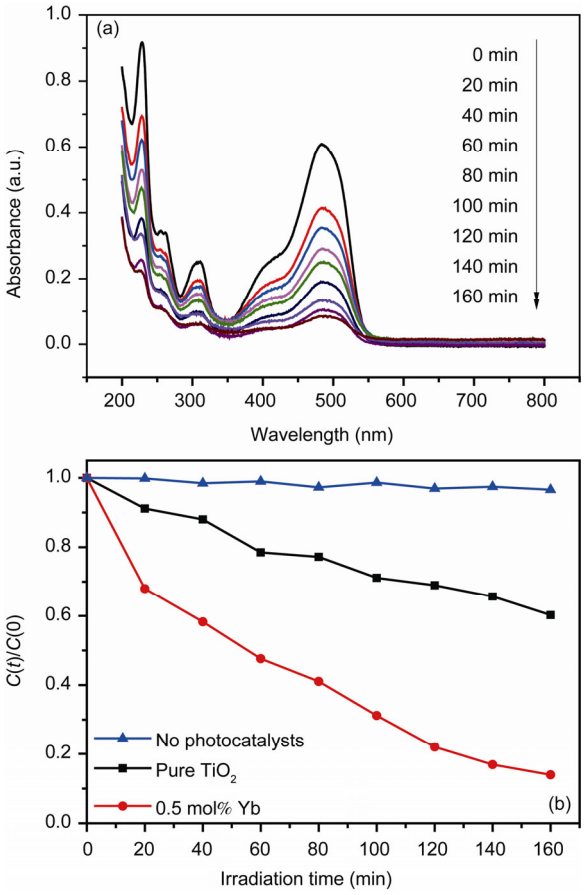

Figure 4 (a) Time-dependent absorption spectra of the Orange II reaction solution in the presence of 0.5 mol% Yb^{3+}-doped TiO_2 HNPs calcinated at 500 °C; (b) plot of $C(t)/C(0)$ against the reaction time in the presence of 0.5 mol% Yb^{3+}-doped TiO_2 HNPs and pure TiO_2 HNPs calcinated at 500 °C.

which means that the recombination of electron and holes can be inhibited. The recombination of the electrons and holes in semiconductor thus become more difficult. These results demonstrate that the Yb^{3+} doping can enhance the

photocatalytic activity of TiO_2 HNPs and improve the utilization efficiency of solar energy.

These Yb^{3+}-doped TiO_2 HNPs were then utilized as photoanodes for dye-sensitized solar cells (DSSCs) application. A DSSC device is essentially a photoelectrochemical system (Figure 5(a)) consisting of two electrodes: N719 dye molecules are adsorbed onto the surface of Yb^{3+}-doped TiO_2 HNPs samples and a redox-coupled electrolyte containing iodide and triiodide ions (I^-/I_3^-). One of the electrodes is the so-called working electrode or photoanode, in which transparent FTO glass is covered with Yb^{3+}-doped TiO_2 HNPs; the other electrode is a counter-electrode of FTO coated with Pt nanoparticles. The photocurrent density-voltage (*J*-*V*) characteristics of all the devices measured under a one-sun condition that correspond to the spectral distribution of standard air mass 1.5 global (AM 1.5 G) and an intensity I_s=100 mW/cm^2 are given in Figure 5(b). Their detailed solar cell parameters as derived from the *J*-*V* curves are summarized for comparison in Table 1. It can be seen that DSSC with 0.5 mol% Yb^{3+}-doped TiO_2 HNPs achieved a maximum J_{SC} (short-circuit photocurrent density) of 7.63 mA/cm^2 and a V_{OC} (open-circuit voltage) of 741 mV. The solar energy-to-electricity conversion efficiency (η) listed in Table 1 was evaluated using the following equation [46]:

$$\eta=(FF\cdot J_{SC}\cdot V_{OC})/P_{in} \quad (1)$$

where P_{in} is the incident light power per unit area and *FF* is the fill factor. As shown in Table 1, at first η shows a rising trend from 2.77% to 3.66% with the doping ratio increasing to 0.5 mol%, while η decreases to 1.87% as the doping ratio continues to increase.

In order to further understand the effects of ytterbium doping on the performance of the TiO_2 HNPs-based DSSCs, we measured electrochemical impedance spectroscopy (EIS) (Figure 5(c)). In the open-circuit condition, there is no current in the external circuit, so electrons injected into the photoelectrode film must be recombined by I_3^- ions. Therefore, the photoexcited electrons' lifetime (τ) in photoanodes can

Table 1 Photoelectrochemical parameters of DSSCs employing pure TiO_2 HNPs and Yb^{3+}-doped TiO_2 HNPs with varied Yb^{3+} addition calcinated at 500 °C as photoanodes

Yb ratio (mol%)	J_{SC} (mA/cm^2)	V_{OC} (mV)	*FF*	η (%)
0	6.72	717	0.573	2.77
0.1	7.50	737	0.637	3.52
0.5	7.63	741	0.647	3.66
1	6.35	767	0.638	3.11
5	3.80	769	0.639	1.87

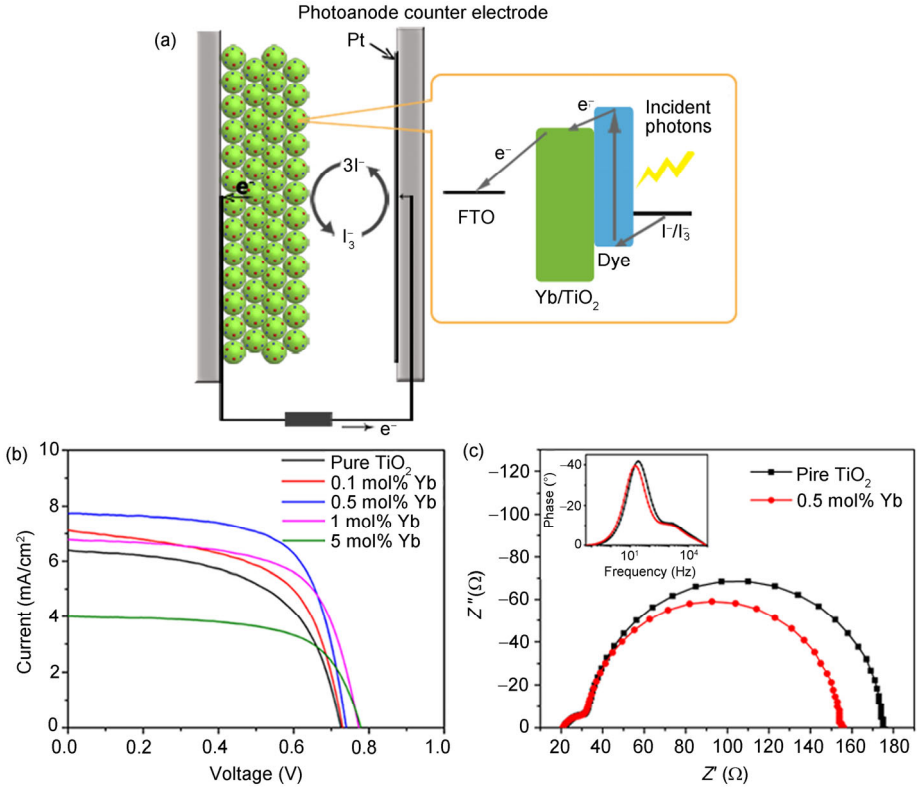

Figure 5 (a) Sketch map of structure of the DSSC device with schematic energy-level diagram; (b) photocurrent density-voltage curves of DSSCs based on pure TiO_2 HNPs and Yb^{3+}-doped TiO_2 HNPs of different doping ratios calcinated at 500 °C; (c) electrochemical impedance spectroscopy (EIS) curves of DSSCs based on pure TiO_2 HNPs and 0.5 mol% Yb^{3+}-doped TiO_2 HNPs calcinated at 500 °C as photoanodes. The inset of (c) displays Bode-phase plots of the two corresponding films.

be estimated by the peak frequency (f_{max}) of the Bode phase plot at middle frequencies [47], according to the following equation:

$$\tau=1/(2\pi f_{max}) \quad (2)$$

Bode phase plots of DSSCs with photoelectrode films of pure TiO_2 HNPs and 0.5 mol% Yb^{3+}-doped TiO_2 HNPs as photoanodes are shown in the inset of Figure 5(c). The f_{max} value in the case of doping Yb^{3+} exhibited a decrease as compared to pure hollow TiO_2. Thus, according to the above analyses, the electron lifetime τ in the photoanode containing 0.5 mol% Yb^{3+} (9.0 ms) is longer than pure hollow TiO_2 electrode (6.1 ms). This result proves that Yb^{3+}-doped hollow TiO_2 facilitates the electron transport, which results from the reduced recombination of injected electrons and decreased diffusive hindrance.

4 Conclusions

We developed a simple and facile route for the preparation of Yb^{3+}-doped TiO_2 single-crystalline hollow nanoparticles based on a general-coordination chemical synthetic strategy via sol-gel method. The obtained Yb^{3+}-doped TiO_2 hollow nanocrystals show a major crystallite size of about 20 nm. The amphiphilic surfactant P123 as the structure-directing agent played a key role in controlling the formation of hollow structure; therefore, we propose a hollow nanostructure growth mechanism. We also demonstrated that by introducing rare-earth ion Yb^{3+} into the synthesis process the obtained products, as photocatalysts, can successfully enhance the photodecomposition efficiency of Orange II azo dye. The obtained Yb^{3+}-doped TiO_2 HNPs were also exploited as photoanodes in DSSCs, and the improvement in photoelectric conversion efficiency was proven by measuring the solar cell parameters of DSSCs under simulative sunlight. The optimal doping ratio we have found results in relatively high photocatalytic and photoelectric conversion efficiencies. These results have great significance in the utilization of solar energy. Therefore, rare-earth doped-titanium hollow-structure nanomaterials have amazing potential in light-harvesting applications such as photocatalysis and dye-sensitized solar cells.

Supporting information

The supporting information is available online at chem.scichina.com and link.springer.com/journal/11426. The supporting materials are published as submitted, without typesetting or editing. The responsibility for scientific accuracy and content remains entirely with the authors.

This work was financially supported by the National Natural Science Foundation of China (21201133, 51272186). Q Yuan thanks Wuhan University for start-up funds and thanks large-scale instrument and equipment sharing foundation of Wuhan University.

1 Hoffmann MR, Martin ST, Choi WY, Bahnemannt DW. Environmental applications of semiconductor photocatalysis. *Chem Rev*, 1995, 95: 69–96
2 Fujishima A, Honda K. Electrochemical photolysis of water at a semiconductor electrode. *Nature,* 1972, 238: 37–38
3 Grätzel M. Solar energy conversion by dye-sensitized photovoltaic cells. *Inorg Chem*, 2005, 44: 6841–6851
4 Yin ZY, Zhu JX, He QY, Cao XH, Tan CL, Chen HY, Yan QY, Zhang H. Graphene-based materials for solar cell applications. *Adv Energy Mater*, 2014, 4: 1300574
5 Zhu JX, Yang D, Yin ZY, Yan QY, Zhang H. Graphene and graphene-based materials for energy storage applications. *Small*, 2014, 10: 3480–3498
6 Mor GK, Shankar K, Paulose M, Varghese OK, Grimes CA. Use of highly-ordered TiO_2 nanotube arrays in dye-sensitized solar cells. *Nano Lett*, 2006, 6: 215–218
7 Hagfeldt A, Boschloo G, Sun L, Kloo L, Pettersson H. Dye-sensitized solar cells. *Chem Rev*, 2012, 110: 6595–6663
8 Chen XB, Liu L, Yu PY, Mao SS. Increasing solar absorption for photocatalysis with black hydrogenated titanium dioxide nanocrystals. *Science*, 2011, 331: 746–750
9 Linsebigler AL, Lu GQ, Yates JT. Photocatalysis on TiO_2 surfaces: principles, mechanisms, and selected results. *Chem Rev*, 1995, 95: 735–758
10 Janisch R, Gopal P, Spaldin NA. Transition metal-doped TiO_2 and ZnO-present status of the field. *J Phys: Condens Matter*, 2005, 17: 657–689
11 Dozzi MV, Selli E. Doping TiO_2 with p-block elements: effects on photocatalytic activity. *J Photochem Photobiol C*, 2013, 14: 13–28
12 Bingham S, Daoud WA. Recent advances in making nano-sized TiO_2 visible-light active through rare-earth metal doping. *J Mater Chem*, 2011, 21: 2041–2050
13 Sandoval S, Yang J, Alfaro JG, Liberman A, Makale M, Chiang CE, Schuller IK, Kummel AC, Trogler WC. Europium-doped TiO_2 hollow nanoshells: two-photon imaging of cell binding. *Chem Mater*, 2012, 24: 4222–4230
14 Frindell KL, Bartl MH, Popitsch A, Stucky GD. Sensitized luminescence of trivalent europium by three-dimensionally arranged anatase nanocrystals in mesostructured titania thin films. *Angew Chem Int Ed*, 2002, 41: 959–962
15 Li L, Tsung CK, Yang Z, Stucky GD, Sun LD, Wang JF, Yan CH. Rare-earth-doped nanocrystalline titania microspheres emitting luminescence via energy transfer. *Adv Mater*, 2008, 20: 903–908
16 Li ZX, Shi FB, Zhang T, Wu HS, Sun LD, Yan CH. Ytterbium stabilized ordered mesoporous titania for near-infrared photocatalysis. *Chem Commun*, 2011, 47: 8109–8111
17 Xu AW, Gao Y, Liu HQ. The preparation, characterization, and their photocatalytic activities of rare-earth-doped TiO_2 nanoparticles. *J Catal*, 2002, 207: 151–157
18 Zhang J, Peng WQ, Chen ZH, Chen H, Han LY. Effect of cerium doping in the TiO_2 photoanode on the electron transport of dye-sensitized solar cells. *J Phys Chem C*, 2012, 116: 19182–19190
19 Shankar K, Bandara J, Paulose M, Wietasch H, Varghese OK, Mor GK, LaTempa TJ, Thelakkat M, Grimes CA. Highly efficient solar cells using TiO_2 nanotube arrays sensitized with a donor-antenna dye. *Nano Lett*, 2008, 8: 1654–1659
20 Chen XB, Mao SS. Titanium dioxide nanomaterials: synthesis, properties, modifications, and applications. *Chem Rev*, 2007, 107: 2891–2959
21 Lou XW, Archer LA, Yang ZC. Hollow micro-/nanostructures: synthesis and applications. *Adv Mater*, 2008, 20: 3987–4019
22 Kim SW, Kim M, Lee WY, Hyeon T. Fabrication of hollow palladium spheres and their successful application to the recyclable heterogeneous catalyst for Suzuki coupling reactions. *J Am Chem Soc*, 2002, 124: 7642–7643

23 Yang ZZ, Niu ZW, Lu YF, Hu ZB, Han CC. Templated synthesis of inorganic hollow spheres with a tunable cavity size onto core-shell gel particles. *Angew Chem Int Ed*, 2003, 42: 1943–1945

24 Wang ZY, Lou XW. TiO_2 nanocages: fast synthesis, interior functionalization and improved lithium storage properties. *Adv Mater*, 2012, 24: 4124–4129

25 Wang YW, Xu H, Wang XB, Zhang X, Jia HM, Zhang LZ, Qiu JR. A general approach to porous crystalline TiO_2, $SrTiO_3$, and $BaTiO_3$ spheres. *J Phys Chem B*, 2006, 110: 13835–13840

26 Li HX, Bian ZF, Zhu J, Zhang DQ, Li GS, Huo YN, Li H, Lu YF. Mesoporous titania spheres with tunable chamber stucture and enhanced photocatalytic activity. *J Am Chem Soc*, 2007, 129: 8406–8407

27 Lou XW, Archer LA. A general route to nonspherical anatase TiO_2 hollow colloids and magnetic multifunctional particles. *Adv Mater*, 2008, 20: 1853–1858

28 Yang HG, Zeng HC. Preparation of hollow anatase TiO_2 nanospheres via Ostwald ripening. *J Phys Chem B*, 2004, 108: 3492–3495

29 Adachi M, Murata Y, Takao J, Jiu JT, Sakamoto M, Wang FM. Highly efficient dye-sensitized solar cells with a titania thin-film electrode composed of a network structure of single-crystal-like TiO_2 nanowires made by the "oriented attachment" mechanism. *J Am Chem Soc*, 2004, 126: 14943–14949

30 Park C, Yoon J, Thomas EL. Enabling nanotechnology with self-assembled block copolymer patterns. *Polymer*, 2003, 44: 6725– 6760

31 Kim BJ, Bang J, Hawer CJ, Kramer EJ. Effect of areal chain density on the location of polymer-modified gold nanoparticles in a block copolymer template. *Macromolecules*, 2006, 39: 4108–4114

32 Beck JS, Vartuli JC, Roth WJ, Lenowicz ME, Kresge CT, Schmidt KD, Chu CTW, Olson DH, Sheppard EW, McCullen SB, Higgins JB, Schlenker JL. A new family of mesoporous molecular sieves prepared with liquid crystal templates. *J Am Chem Soc*, 1992, 114: 10834–10843

33 Firouzi A, Kumar D, Bull LM, Besier T, Sieger P, Huo Q, Walker SA, Zasadzinski JA, Glinka C, Nicol J, Margolese D, Stucky GD, Chmelka BF, Kumar D. Cooperative organization of inorganic-surfactant and biomimetic assemblies. *Science*, 1995, 267: 1138–1143

34 Förster S, Antonietti M. Amphiphilic block copolymers in structure-controlled nanomaterial hybrids. *Adv Mater*, 1998, 10: 195–217

35 Sasidharan M, Nakashima K, Gunawardhana N, Yokoi T, Inoue M, Yusa S, Yoshio M, Tatsumi T. Novel titania hollow nanospheres of size 28±1 nm using soft-templates and their application for lithium-ion rechargeable batteries. *Chem Commun*, 2011, 47: 6921–6923

36 Soler-Illia GJAA, Sanchez C, Lebeau B, Patarin J. Chemical strategies to design textured materials: from microporous and mesoporous oxides to nanonetworks and hierarchical structures. *Chem Rev*, 2002, 102: 4093–4138

37 Alexandridis P, Holzwarth JF. Differential scanning calorimetry investigation of the effect of salts on aqueous solution properties of an amphiphilic block copolymer (Poloxamer). *Langmuir*, 1997, 13: 6074–6082

38 Pandit N, Trygstad T, Croy S, Bohorquez M, Koch C. Effect of salts on the micellization, clouding, and solubilization behavior of pluronic F127 solutions. *J Colloid Interface Sci*, 2000, 222: 213–220

39 Yang P, Zhao D, Margolese DI, Chmelka BF, Stucky GD. Block copolymer templating syntheses of mesoporous metal oxides with large ordering lengths and semicrystalline framework. *Chem Mater*, 1999, 11: 2813–2826

40 Zhao DY, Feng JL, Huo QS, Melosh N, Fredrickson GH, Chmelka BF, Stucky GD. Triblock copolymer syntheses of mesoporous silica with periodic 50 to 300 angstrom pores. *Science*, 1998, 279: 548–552

41 Samiee L, Beitollahi A, Bahmani M, Akbarnejad MM, Vinu A. Effects of ageing conditions and block copolymer concentration on the stability and micellization of P123-Ti^{4+} sols prepared by the templating method. *Res Chem Intermed*, 2010, 36: 897–923

42 Yang PD, Zhao DY, Margolese DI, Chmelka BF, Stucky GD. Generalized syntheses of large-pore mesoporous metal oxides with semicrystalline frameworks. *Nature*, 1998, 396: 152–155

43 Seebergh JE, Berg JC. Depletion flocculation of aqueous, electrosterically-stabilized latex dispersions. *Langmuir*, 1994, 10: 454–463

44 Štengl V, Bakardjieva S, Murafa N. Preparation and photocatalytic activity of rare earth doped TiO_2 nanoparticles. *Mater Chem Phys*, 2009, 114: 217–226

45 Wang C, Ao YH, Wang PF, Hou J, Qian J. Preparation, characterization and photocatalytic activity of the neodymium-doped TiO_2 hollow spheres. *Appl Surf Sci*, 2010, 257: 227–231

46 Fan K, Zhang W, Peng TY, Chen JN, Yang F. Application of TiO_2 fusiform nanorods for dye-sensitized solar cells with significantly improved efficiency. *J Phys Chem C*, 2011, 115: 17213–17219

47 Liang LL, Liu YM, Bu CH, Guo KM, Sun WW, Huang N, Peng T, Sebo B, Pan MM, Liu W, Guo SS, Zhao XZ. Highly uniform, bifunctional core/double-shell-structured β-$NaYF_4$:Er^{3+}, Yb^{3+}@SiO_2@TiO_2 hexagonal sub-microprisms for high-performance dye sensitized solar cells. *Adv Mater*, 2013, 25: 2174–2180